Cellular and Molecular Life Sciences (2018) 75:2473–2488
https://doi.org/10.1007/s00018-017-2742-3

ORIGINAL ARTICLE

Furin promotes dendritic morphogenesis and learning and memory in transgenic mice

Binglin Zhu[1] · Lige Zhao[1] · Dong Luo[1] · Demei Xu[1] · Tao Tan[2] · Zhifang Dong[2] · Ying Tang[1] · Zhuo Min[1] · Xiaojuan Deng[1] · Fei Sun[3] · Zhen Yan[4] · Guojun Chen[1]

Received: 22 September 2017 / Revised: 30 November 2017 / Accepted: 27 December 2017 / Published online: 4 January 2018

Abstract

Furin is a proprotein convertase implicated in a variety of pathological processes including neurodegenerative diseases. However, the role of furin in neuronal plasticity and learning and memory remains to be elucidated. Here, we report that in brain-specific furin transgenic (Furin-Tg) mice, the dendritic spine density and proliferation of neural progenitor cells were significantly increased. These mice exhibited enhanced long-term potentiation (LTP) and spatial learning and memory performance, without alterations of miniature excitatory/inhibitory postsynaptic currents. In the cortex and hippocampus of Furin-Tg mice, the ratio of mature brain-derived neurotrophic factor (mBDNF) to pro-BDNF, and the activities of extracellular signal-related kinase (ERK) and cAMP response element-binding protein (CREB) were significantly elevated. We also found that hippocampal knockdown of CREB diminished the facilitation of LTP and cognitive function in Furin-Tg mice. Together, our results demonstrate that furin enhances dendritic morphogenesis and learning and memory in transgenic mice, which may be associated with BDNF–ERK–CREB signaling pathway.

Keywords Furin · BDNF · CREB · Learning and memory · Long-term potentiation (LTP)

Introduction

Furin is a proprotein convertase (PC) that catalyzes the proteolytic maturation of proprotein substrates in the secretory pathway. In the living cell, furin cycles between trans-Golgi network (TGN), the cell surface and the early endosome [1], where it cleaves a variety of substrates including precursors of growth receptors and hormones, matrix metalloproteinases, viral envelope glycoproteins and bacterial exotoxins [2]. Furin knockout mice are unable to survive due to cardiac developmental defects at 10.5 embryonic days [3]. It is suggested that furin plays an important role in homeostasis as well as in diseases including Alzheimer's disease, cancer, anthrax and Ebola fever [1].

In *C. elegans*, furin promotes differentiation and collateral formation of sensory neurons [4, 5]. Evidence has suggested that furin regulates neuronal function through brain-derived neurotrophic factor (BDNF) [6, 7]. For instance, in rat astrocytes exposed to oxygen–glucose deprivation, furin mediates BDNF upregulation [8]. BDNF receptor activation requires intracellular proteolysis of pro-BDNF by furin [9]. While mature BDNF (mBDNF) plays critical role in the development and survival of neurons [10], pro-BDNF inhibits its synaptic plasticity [11]. In the mammalian hippocampus, BDNF has emerged as a key regulator of synaptic plasticity and long-term potentiation (LTP) [12, 13]. The latter is widely considered as the cellular mechanism underlying learning and memory [14–16].

We hypothesized that in mammals, furin may regulate neuronal development and learning and memory. We found

✉ Guojun Chen
woodchen2015@163.com

[1] Department of Neurology, The First Affiliated Hospital of Chongqing Medical University, Chongqing Key Laboratory of Neurology, 1 Youyi Road, Chongqing 400016, China

[2] Chongqing Key Laboratory of Translational Medical Research in Cognitive Development and Learning and Memory Disorders, Ministry of Education Key Laboratory of Child Development and Disorders, Children's Hospital of Chongqing Medical University, 136 Zhongshan Er Lu, Chongqing 400014, China

[3] Department of Physiology, Wayne State University School of Medicine, Detroit, MI 48201, USA

[4] Department of Physiology and Biophysics, State University of New York at Buffalo, Buffalo, NY 14214, USA

that in furin transgenic (Tg) mice, spine morphogenesis, LTP and spatial memory performance were enhanced, with the concomitant increase of the ratio of mBDNF/pro-BDNF and associated extracellular signal-related kinase (ERK) and cAMP response element-binding protein (CREB) activities. We further found that hippocampal knockdown of CREB reduced furin regulation of LTP and memory performance.

Materials and methods

Animals

To generate a line of transgenic mice that overexpress furin in the brain, we constructed a transcription unit by inserting the coding region of the mouse *furin* cDNA into the MoPrP (mouse prion gene promoter)-polyA cassette. This vector was used here because it enabled relatively high levels of transgene expression in central nervous system (CNS) neurons [17]. The linearized MoPrP-*furin* transcription unit was microinjected into fertilized eggs of C57BL/6J mice that were then transferred to the oviducts of pseudopregnant females (CasGene Biotech Co., Ltd, Beijing, China). The transgenic founder mice were obtained and crossed to C57BL/6J wild-type mice (WT) to establish transgenic lines. All animal handling procedures followed the guidelines for Laboratory Animal Research of Chongqing Medical University. The use of animals was approved by the Institutional Animal Care and Use Committee of Chongqing Medical University. The mice (2- to 3-month-old) were maintained in a constant environmental condition (temperature 23 ± 2 °C, humidity 55 ± 5%, and 12:12 h light/dark cycle). Furin transgenic mice (Tg, male) were confirmed by PCR genotyping with the following primer sequences: 5′-GACCAC ATGACTACTCTGCTGATGGG-3′ and 5′-TCAAAGGGC GCTCTGGTC TTTG-3′.

Lentiviral vector and intrahippocampal microinjection

The recombinant lentiviral vector of mouse *CREB* shRNA, along with the transgene for green fluorescent protein (GFP), was produced by Shanghai GeneChem Co., Ltd. (Shanghai, China). A universal scrambled sequence with mismatched bases was used as a control. The control shRNA (lenti-scr) targeting sequence is 5′-UUCUCCGAA CGUGUCACGU-3′; the sequence of *CREB* shRNA (lenti-shCREB) was 5′-AUACAGCUGGCUAACAAUGG-3′ [18]. WT and Tg mice were injected bilaterally into dorsal hippocampus with lenti-shCREB or lenti-scr. The method of intrahippocampus injection was carried out as previously described with minor modification [19]. In brief, WT and Tg mice (8–12 weeks of age) were deeply anesthetized by intraperitoneal injection of 3.5% chloral hydrate (0.01 mL/g) and mounted on a stereotaxic frame (Stoelting Co. Ltd., USA). The lentiviral particles (2×10^8 TU/mL in 3 μL) containing empty vector or CREB were microinjected bilaterally into the dorsal hippocampus (anteroposterior (AP), − 2.0 mm; mediolateral (ML), − 1.8 mm; dorsoventral (DV), − 2.3 mm) using a glass pipette at a speed of 0.2 μL/min. To prevent backflow of viral particles, the pipette was kept in place for 5 min after injection. Two weeks after injection, mice were tested on Morris water maze and electrophysiological recordings, and then tissue were collected for Western blotting analysis.

Anti-BDNF antibody injection was performed as previously described [20, 21]. The rabbit anti-BDNF and control rabbit IgG antibodies were purchased from Proteintech (Wuhan, China) and dissolved in 1× PBS and injected at 0.5 μg per injection per side (the dosage of BDNF has been used to disrupt long-term memory consolidation when injected into the hippocampus) [22]. 2 days after the injection, hippocampus tissues were harvested and subjected to Western blotting analysis and brain slices were prepared for electrophysiological recordings.

Western blotting

Isolated samples from the hippocampus, cortex, midbrain, cerebellum, olfactory bulb, spleen, liver and kidney of mice were homogenized in RIPA buffer (Beyotime, Haimen, China) supplemented with protease inhibitors (complete Mini, Roche, Indianapolis, USA). Western blot analysis was performed as described previously [23]. Protein concentrations were measured using a BCA assay (Dingguo, Beijing, China). Protein samples were separated on a 8% Bis–Tris gel, transferred to a PVDF membrane (Millipore, Billerica, MA, USA) and probed with the antibodies against furin (1:2000, Abcam, Cambridge, UK), PSD95 (1:1000, Proteintech, Wuhan, China), CREB (1:2000, Abcam), phosphor-CREB (1:2000, p-CREB, Abcam), CaMKII (1:3000, Abcam), phosphor-CaMKII (1:2000, p-CaMKII, Abcam), ERK1/2 (1:3000, Abcam), phosphor-ERK1/2 (1:2000, p-ERK1/2, Abcam), BDNF (1:500, Proteintech) and GAPDH (1:10,000, Proteintech) overnight at 4 °C. The blots were washed and incubated for 1 h with HRP-conjugated anti-rabbit or anti-mouse secondary antibodies (1:5000, Proteintech). Bands were visualized using an ECL reagent (Thermo, Marina, USA) and Fusion FX5 analysis system (Vilber Lourmat, Marnela-Vallée, France). Relative expression levels were calculated using the Quantity One software (Bio-Rad, Hercules, USA) with normalization to the GAPDH signal.

Immunohistochemistry (IHC)

The brain tissue sections from WT and Tg mice were formalin-fixed and embedded in paraffin, and then sections were deparaffinized in xylene and rehydrated in a graded series of ethanol before staining. After antigen retrieval and blocking, the sections were then incubated with anti-furin antibody (1:100, Abcam) at 4 °C overnight. The second day, after washing with PBS sections were incubated with a biotinylated secondary goat anti-rabbit antibody (1:500, Zhongshan Golden Bridge, Inc.) for 30 min at 37 °C, and then incubated with an avidin–biotin–peroxidase complex (Zhongshan Golden Bridge) for 30 min at 37 °C. The sections were washed in PBS and incubated with 3,3′-diaminobenzidine (DAB, Zhongshan Golden Bridge) for 3 min. Hematoxylin was used to counterstain nuclei. A LEICA DM6000B automatic microscope (Leica, Germany) was used to collect images. Ten random visual field images for every section were analyzed automatically and semiquantitatively using the Motic Med 6.0 CMIAS pathology image analysis system (Beijing Motic, Beijing, China).

Real-time quantitative PCR

Frozen tissue from all WT and Tg mice were sonicated in a 1:20 w/v ratio in TRIzol (Takara, Dalian, China) according to the manufacturer's protocol. cDNA synthesis was performed using a PrimeScript RT reagent kit (Vazyme, Nanjing, China). The expression of *furin* mRNA was detected by quantitative real-time PCR (qPCR) and reactions were performed on a Bio-Rad IQ™5 detection system (Bio-Rad) with an SYBR green master mix (Takara). The sequences of the primers were as follows: *furin*: 5′-TGCCACGCC TCATGTGCC-3′ and 5′-GCTCTGGCTTTGCCGGGA -3′; *GAPDH*: 5′-TTGTCATGGGAGTGAACGAGA-3′ and 5′-CAGGCAGTTGGTGGTACAGG-3′. The reaction mixture (20 µL total) consisted of 10 µL 2× SYBR mix, 7.2 µL nuclease-free water, 0.4 µL each primer (10 µM) and 2 µL diluted cDNA. The reaction program was performed using the following steps: 95 °C 30 s, followed by 40 cycles (95 °C for 5 s, 60 °C for 10 s and 72 °C for 15 s). At the end of the cycling process, the temperature was raised from 60 to 95 °C to obtain the melting curve. Each reaction was performed in triplicate for each sample, and the average cycle threshold value (Ct) for housekeeping gene *GAPDH* was used to normalize the raw cycle threshold data and calculate ΔCt. The fold changes were quantified using the $2^{-\Delta\Delta Ct}$ method [$\Delta\Delta Ct = (Ct_{furin} - Ct_{GAPDH})_{Tg} - (Ct_{furin} - Ct_{GAPDH})_{WT}$].

Golgi–Cox staining

Golgi–Cox staining was conducted using the FD Rapid GolgiStain Kit (FD Neuro-technologies, Ellicott City, MD, USA) according to the manufacturer's instructions. Mice were perfused intracardially with phosphate buffer under deep sodium pentobarbital anesthesia. Whole brain tissues were rapidly removed from mice and immersed into Golgi–Cox solution A and B for 2 weeks in the dark, and then transferred to solution C for 72 h at 4 °C. Slices of 100 µm thick were cut at − 20 °C using a cryostat microtome (Leica CM1950 cryostat, Leica, Germany). For Golgi–Cox staining, the sections were mounted on 3% gelatin-coated glass slides, air-dried for 7 days and then stained with solutions D and E followed by alcohol dehydration, then cleared with xylene and mounted using a resinous medium. Dendritic spines were imaged using a 100× objective oil immersion lens and captured with a Leica DFC 280 digital camera (Tokyo, Japan). For density of dendritic spine quantification, dendritic segments in CA1 region of the hippocampus were randomly selected and the counting was carried out by an experimenter blinded to the group of each sample.

BrdU labeling

To assess cellular proliferation of neurons, WT and Tg mice were given a single intraperitoneal injection of bromodeoxyuridine (BrdU, Sigma, 50 mg/kg, 0.1 M NaOH, NaCl 0.9%) per day for four consecutive days. Animals were killed 24 h after last BrdU injection, and perfused with 0.9% NaCl followed by 4% paraformaldehyde (PFA). Brain sections (30 µm) were treated with 2 M HCl for 20 min, 4% $Na_2B_4O_7$ for 10 min, blocked with 10% normal goat serum at 37 °C for 30 min, and incubated with rabbit anti-BrdU antibody (GeneTex) and goat anti-doublecortin antibody (DCX, Santa Cruz Biotechnology) overnight at 4 °C. The sections were washed and incubated with Alexa Fluor-488 donkey anti-goat IgG (Abbkine, California, USA) or Alexa Fluor-555 donkey anti-rabbit IgG (Beyotime, Haimen, China) at 37 °C for 1 h. Sections were rinsed, mounted with Vectashield (Vector Labs) and visualized with confocal laser scanning microscopy (Leica, Wetzlar, Germany). Quantification of labeled cells was performed with Image J software.

Morris water maze

Morris water maze testing procedure was carried out in a circular swimming pool as previously described [24]. In training session, mice performed four trials per day for five consecutive days. They were allowed to swim for up to 60 s until the platform was found. If mice failed find the platform within the given time, they were gently guided to rest there for 10 s. The escape latency was recorded in each training session. In probe trials on the sixth day, the platform was removed, and each mouse was given 60 s to locate where the platform was originally placed. The time spent in target quadrant and the times of platform crossings were measured.

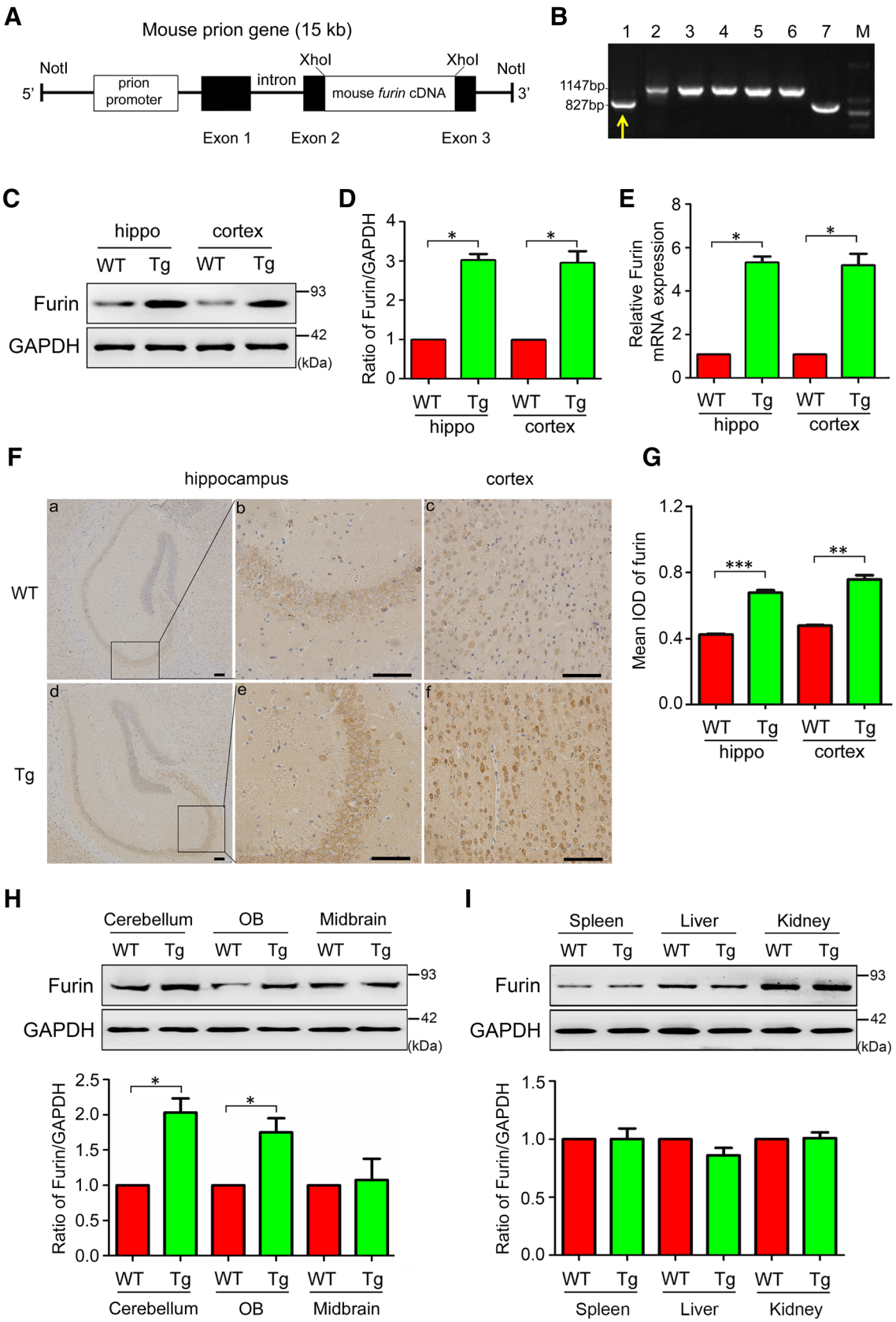
A
Mouse prion gene (15 kb)
NotI
prion promoter
intron
XhoI
mouse furin cDNA
XhoI
NotI
5'
3'
Exon 1
Exon 2
Exon 3
B
1 2 3 4 5 6 7 M
1147bp
827bp
C
hippo
cortex
WT Tg WT Tg
Furin
GAPDH
93
42
(kDa)
D
Ratio of Furin/GAPDH
WT Tg WT Tg
hippo
cortex
E
Relative Furin mRNA expression
WT Tg WT Tg
hippo
cortex
F
hippocampus
cortex
WT
Tg
a
b
c
d
e
f
G
Mean IOD of furin
WT Tg WT Tg
hippo
cortex
H
Cerebellum
OB
Midbrain
WT Tg WT Tg WT Tg
Furin
GAPDH
93
42
(kDa)
Ratio of Furin/GAPDH
WT Tg WT Tg WT Tg
Cerebellum
OB
Midbrain
I
Spleen
Liver
Kidney
WT Tg WT Tg WT Tg
Furin
GAPDH
93
42
(kDa)
Ratio of Furin/GAPDH
WT Tg WT Tg WT Tg
Spleen
Liver
Kidney

◂**Fig. 1** Furin expression is significantly increased in transgenic mice. **A** Schematic of furin construct. Full-length cDNA for mouse *furin* was cloned into MoPrP vector. **B** Germline transmission of the transgene was checked by PCR analysis of tail DNA using transgenic primers. 1–6, tail snip genomic DNA; 7, positive control vector DNA; M, DNA molecular weight standards. Yellow arrow indicated MoPrP-furin/+. Representative Western blots (**C**) and quantification (**D**) of furin protein levels in the hippocampus (hippo) and cortex in wild-type (WT) and furin transgenic (Tg) mice, respectively (data were analyzed by Student's *t* test; $n = 6$. Error bars are SEM; $^*P < 0.05$). The molecular weight of protein marker in kDa is shown to the right of each Western blot panel. **E** mRNA level of *furin* was determined by real-time PCR in WT and Tg mice (data were analyzed by Student's *t* test; $n = 6$. Error bars are SEM; $^*P < 0.05$). **F** Representative immunohistochemistry images from WT and Tg mice (a–f). Expression of furin is in the cytoplasm of neurons in the hippocampus (a, d) and cortex (c, f). Magnification of the marked area is shown (b, e). Scale bar: 100 μm. **G** A bar graph of the mean integral optical density (IOD) of furin shows a significant increase in the hippocampus (hippo) and cortex in Tg mice compared to WT mice. Data represent the mean ± SEM of four slices per genotype. $^{**}P < 0.01$, $^{***}P < 0.001$ using Student's *t* test. **H** Representative Western blot and quantification of furin protein level normalized to GAPDH in the cerebellum, olfactory bulb (OB) and midbrain from WT and Tg mice (data were analyzed by Student's *t* test; $n = 6$. Error bars are SEM; $^*P < 0.05$). **I** Representative Western blot and quantification of furin protein level normalized to GAPDH in the spleen, liver and kidney from WT and Tg mice (data were analyzed by Student's *t* test; $n = 6$. Error bars are SEM)

Performance was video-recorded and analyzed by image analyzing software (ANY-maze; Stoelting Co., Wood Dale, USA).

Electrophysiological recordings

Brain slices were prepared as described previously [25, 26]. The hippocampal slices (400 μm) were prepared with a Leica (Germany) VP1200S Vibratome and then incubated in artificial cerebral spinal fluid (ACSF) containing (in mM) 124 NaCl, 26 $NaHCO_3$, 0.4 Na-vitamin C, 2 pyruvate-Na, 2 lactate-Na, 2.8 KCl, 1.25 $NaH_2PO_4{\cdot}2H_2O$, 1.2 $MgSO_4$, 2 $CaCl_2$ and 10 D-glucose (pH 7.4, 310 mOsm/L) at 32 °C saturated with 95% O_2 and 5% CO_2 for at least 1 h before recording.

Field excitatory postsynaptic potentials (fEPSPs) were recorded using borosilicate glass pipettes filled with ACSF at a frequency of 0.033 Hz. A bipolar stimulating electrode (100 μm in diameter) was inserted into stratum radiatum of the CA1 region to stimulate the Schaffer collateral pathway, and a unipolar recording electrode (1- to 2-μm tip) filled with 3 M NaCl was used for recording [27]. The test stimulation intensity was adjusted to 50–80% of the maximal fEPSP amplitude ranging from 80 to 200 μA (baseline stimulation). After recording stable baseline fEPSP responses for 30 min, long-term potentiation (LTP) was induced by a high-frequency stimulation (HFS; 100 Hz for 1 s) and then the fEPSPs were continuously recorded for 1 h.

mEPSCs were recorded in voltage clamp at a membrane potential of − 70 mV in the presence of 1 μM tetrodotoxin (TTX) and 100 μM picrotoxin (PTX) using an intracellular solution composed of the following (in mM): 130 Cs-methanesulfonate, 10 HEPES, 10 CsCl, 4 NaCl, 1 $MgCl_2$, 1 EGTA, 5 NMG, 5 MgATP, 0.5 Na_2GTP and 12 phosphocreatine (pH 7.2, 275–290 mOsm/L). Recording of mIPSCs was carried out at a membrane voltage of − 70 mV in the presence of 1 μM TTX, 10 μM 6,7-dinitroquinoxaline-2,3(1H,4H)-dione (DNQX) and 50 μM DL-2-amino-5-phosphonovaleric acid (DL-APV) using an intracellular solution composed of the following (in mM): 100 CsCl, 10 HEPES, 1 $MgCl_2$, 1 EGTA, 30 *N*-methyl-D-glucamine (NMG), 5 MgATP, 0.5 Na_2GTP, 12 phosphocreatine (pH 7.2–7.3, 270–280 mOsm/L). mEPSCs and mIPSCs were analyzed using Mini Analysis 6.0.1 and Clampfit10.3.

Statistical analysis

In the Morris water maze test, a mixed analysis of variance (ANOVA) analysis was performed to analyze the escape latencies to find the platform during training sessions. The statistical differences between groups were analyzed using Student's *t* test. All data in the figures are presented as the mean ± SEM, and $P < 0.05$ is considered statistically significant.

Results

Verification of furin transgenic mice

We generated furin transgenic (Tg) mice using the MoPrP promoter to drive expression of full-length, wild-type mouse *furin* (Fig. 1A). Genotyping involved extracting genomic DNA from mouse tails and carrying out PCR with Tg primers, producing either a 1147-bp (containing two introns) or 827-bp (introns deletion, MoPrP-furin/+) PCR product (Fig. 1B). Compared to WT mice, Tg mice showed an increase of furin protein (Fig. 1C, D) and mRNA expression (Fig. 1E). Immunohistochemical results showed that furin protein was expressed primarily in the cytoplasm of neurons in hippocampus and cortex of WT and Tg mice (Fig. 1F). Student's *t* test revealed that the mean integral optical density (IOD) of furin was significantly higher in the hippocampus ($P < 0.001$) and cortex ($P < 0.01$) of Tg mice than in those of WT mice (Fig. 1G). To assess the range of tissues in which furin protein was expressed, the other six different organs (cerebellum, olfactory bulb, midbrain, spleen, liver and kidney) were also harvested and subjected to Western blotting analysis using anti-furin antibody. Results indicated that furin was overexpressed in the cerebellum and olfactory bulb (OB), with no changes in midbrain and peripheral

(spleen, liver and kidney) in Tg mice relative to WT mice (Fig. 1H, I), indicating that the brain-specific transgenic model is successful.

Dendritic spine density was increased in Tg mice

Furin is known to promote dendritic arborization of sensory neurons in *C. elegans* [4, 5], and spine morphogenesis is essential for synaptic plasticity and learning and memory [28, 29]. Thus, we examined whether furin may affect dendritic morphogenesis in CA1 neurons. Representative photomicrographs of dendritic spines in hippocampal CA1 are shown in Fig. 2A. Compared with WT mice, the dendritic spine density in the hippocampal CA1 region of Tg mice was significantly increased (WT: 0.67 ± 0.03/10 μm, $n = 8$; Tg: 0.97 ± 0.02/10 μm, $n = 8$, $P < 0.05$, Fig. 2B). However, no differences were observed in size (WT: 274.35 ± 11.61 μm^2, $n = 40$; Tg: 264.76 ± 8.78 μm^2, $n = 42$, $P > 0.05$, Fig. 2C), perimeter of soma (WT: 68.29 ± 1.56 μm, $n = 40$; Tg: 68.52 ± 1.49 μm, $n = 42$, $P > 0.05$, Fig. 2D), maximum distance from dendritic terminal to soma (WT: 156.36 ± 11.21 μm, $n = 40$; Tg: 162.56 ± 17.16 μm, $n = 42$, $P > 0.05$, Fig. 2E) and number of intersections (WT: 6.84 ± 0.12, $n = 40$; Tg: 8.21 ± 0.2, $n = 42$, $P > 0.05$, Fig. 2F) in the two groups. These results indicated that furin enhanced neuronal spine densities without affecting dendritic arborization.

Neuronal proliferation was enhanced in Tg mice

To further determine whether the increased spine density may be associated with neuronal proliferation, we measured the hippocampal immunostaining of BrdU and DCX, the markers of proliferation and blast/immature neurons, respectively [30]. As shown in Fig. 2G, H, $BrdU^+$ cells were significantly increased in the hippocampus of Tg mice compared with WT mice ($P < 0.05$). Double immunostaining with BrdU and DCX revealed that the number of $BrdU^+$–DCX^+ cells was significantly increased in Tg mice ($P < 0.01$, Fig. 2I). However, the ratio of neuronal differentiation, defined as the proportion of $BrdU^+$–DCX^+ to total $BrdU^+$ cells, was unchanged in the two groups (Fig. 2J). These results indicated that furin positively regulated neural progenitor cells (NPC) proliferation, but did not affect the early differentiation of NPC into immature neurons.

Furin enhanced hippocampal LTP but not synaptic transmission

Long-term potentiation (LTP) is a well-characterized form of synaptic plasticity, which has been considered as a cellular correlate of learning and memory [14–16]. To understand the role of furin in synaptic plasticity, LTP was analyzed in Schaffer Collateral (SC)-CA1 region of hippocampal slices. Following a stable 30-min baseline recording of field excitatory postsynaptic potential (fEPSP), a high-frequency stimulation (HFS; 100 Hz for 1 s) was applied to induce LTP. As shown in Fig. 3A, a strong potentiation was observed in slices of Tg mice compared with WT mice (last 10 min of recording, Tg, 165.5 ± 4.25%; WT, 143.8 ± 4.51%, $n = 6/6$ mice, $P < 0.05$, Fig. 3B). It is reported that LTP involves the functional role of glutamate receptors AMPAR and NMDAR [31]. Thus, we next investigated the influence of furin on synaptic transmission in the CA1 pyramidal neurons. As shown in Fig. 3C–H, the amplitude and frequency of mEPSCs and mIPSCs were not significantly different in both groups ($n = 6/6$ mice). Taken together, these results indicated that furin enhanced hippocampal LTP, but did not affect excitatory/inhibitory synaptic transmission.

Furin improved spatial learning and memory in Tg mice

To further validate that the enhanced LTP is associated with learning and memory, Morris water maze test was used to assess behavioral performances in Tg and WT mice [32]. As shown in Fig. 4A, Tg mice showed significantly shorter escape latency to find the hidden platform compared to WT mice on day 5 (WT: 38.14 ± 2.94 s; Tg: 21.86 ± 2.82 s, $P < 0.001$) and day 6 (WT: 32.82 ± 3.12 s; Tg: 16.45 ± 2.87 s, $P < 0.001$). In the probe trial test, Tg mice exhibited an increased number of platform crossing (WT: 1.61 ± 0.36; Tg: 2.67 ± 0.32, $P < 0.05$, Fig. 4B), and more times spent in the target quadrant (TQ) (WT: 23.46 ± 4.35 s; Tg: 32.04 ± 4.63 s, $P < 0.05$, Fig. 4C) compared to WT mice. Representative probe trial trajectories for both groups are shown (Fig. 4D). These results indicated that furin promoted the learning and memory performance, which was consistent with the LTP enhancement in Tg mice.

mBDNF/proBDNF ratio and CREB phosphorylation were elevated in Tg mice

The molecular mechanisms underlying LTP and memory formation have been intensively studied [33, 34]. Synaptic remodeling, CaMKII, and BDNF–ERK–CREB signaling are considered as the key molecular regulators for synaptic plasticity and memory [35–38]. To validate that the increased spine density in Tg mice is associated with postsynaptic marker PSD95, we first assessed the expression level of PSD95 in the cortex and hippocampus of Tg mice. As expected, PSD95 protein was significantly elevated in the hippocampus ($P < 0.05$) and cortex ($P < 0.01$) of Tg mice, compared with WT mice. In addition, the ratio of mBDNF to pro-BDNF and the phosphorylation of ERK and CREB (p-ERK and p-CREB, respectively) were also consistently

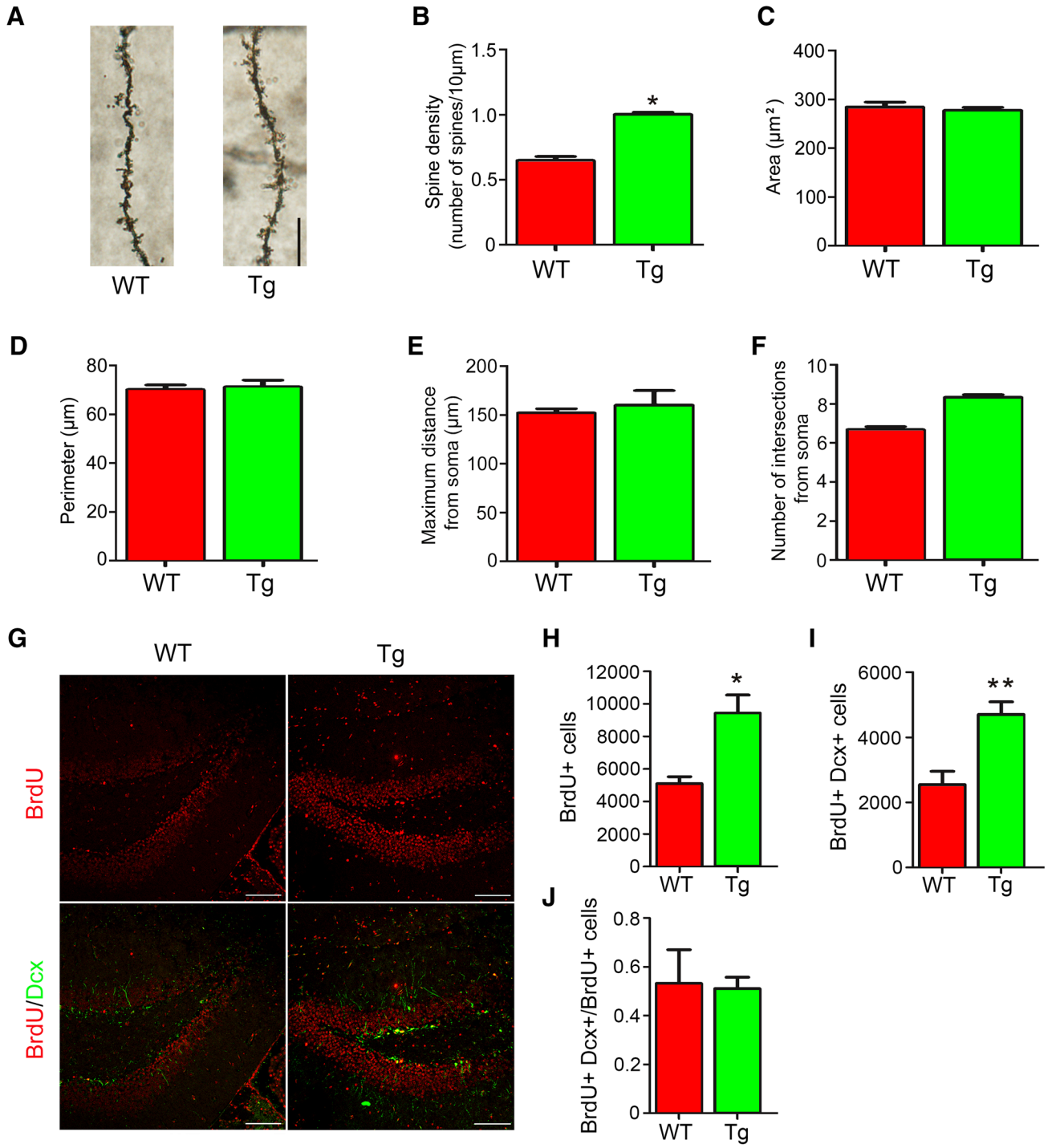

Fig. 2 Furin increases dendritic spine density and neuronal proliferation. **A** Representative photomicrographs of dendritic spines in CA1 area of WT and Tg mice. Scale bar: 5 μm. **B**–**F** Quantification of dendritic spine density (total number per 10 μm) (**B**, $n = 8$ mice in each), size of soma (**C**, $n = 40$ in WT/42 in Tg), perimeter of soma (**D**, $n = 40$ in WT/42 in Tg), maximum distance from dendritic terminal to soma (**E**, $n = 40$ in WT/42 in Tg) and cross number with soma (**F**, $n = 40$ in WT/42 in Tg) in CA1 region of WT and Tg mice (data were analyzed by Student's t test; error bars are SEM; $^*P < 0.05$). **G** Representative confocal microscopic images showing the immunostaining of BrdU (red) and DCX (green) and merged images (yellow) in hippocampal slices from WT and Tg mice, respectively. Scale bar: 100 μm. Quantification of the total number of $BrdU^+$ (**H**) and DCX^+ neurons (**I**) (data were analyzed by Student's t test; $n = 5$. Error bars are SEM; $^*P < 0.05$, $^{**}P < 0.01$). **J** The ratio of $BrdU^+$–DCX^+/total $BrdU^+$ cells is not significantly different between WT and Tg mice (data were analyzed by Student's t test; $n = 5$. Error bars are SEM)

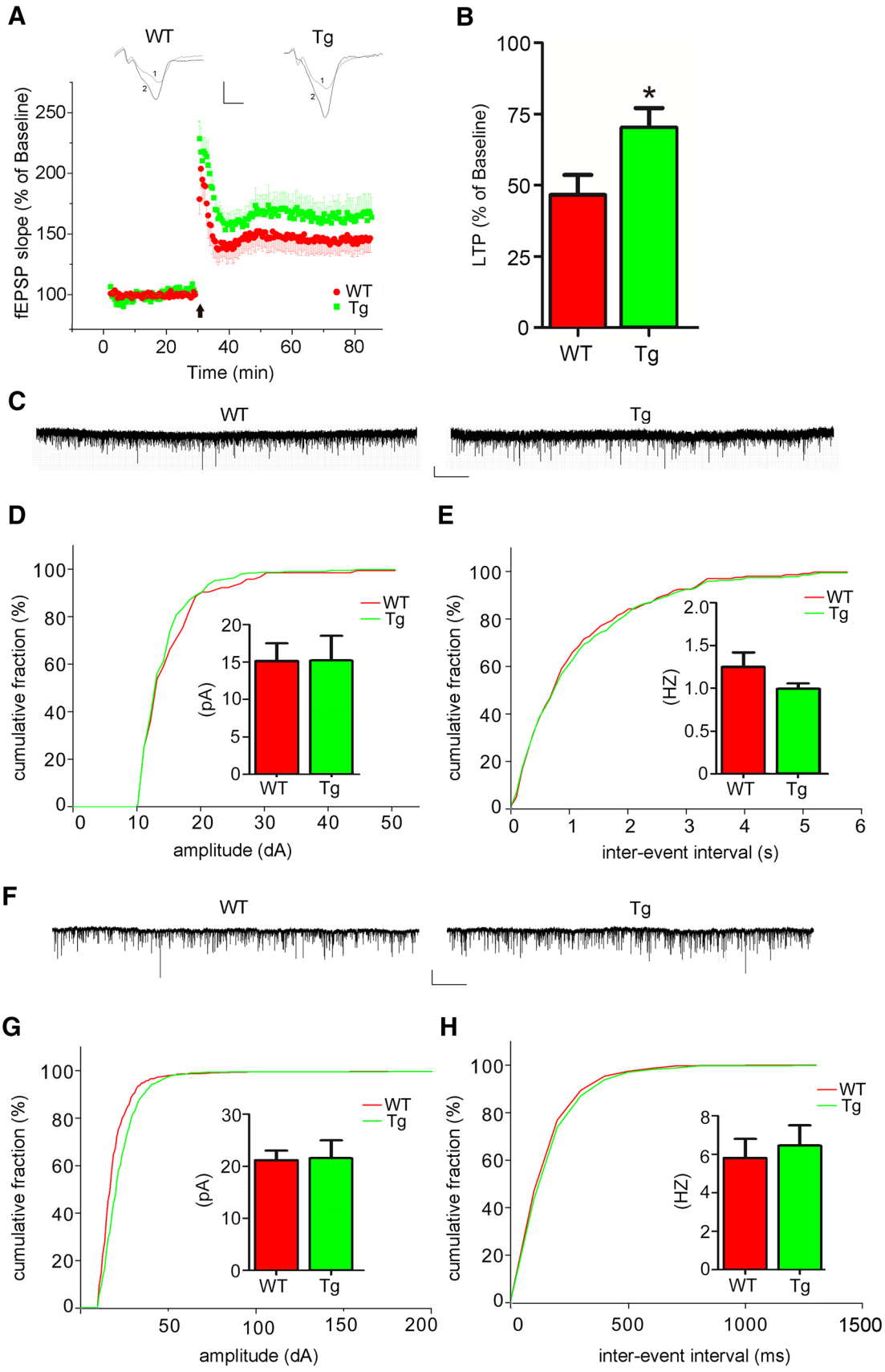
A
WT
Tg
fEPSP slope (% of Baseline)
250
200
150
100
0
20
40
60
80
Time (min)
WT
Tg
B
LTP (% of Baseline)
100
75
50
25
0
*
WT
Tg
C
WT
Tg
D
cumulative fraction (%)
100
80
60
40
20
0
0
10
20
30
40
50
amplitude (dA)
WT
Tg
(pA)
20
15
10
5
0
WT
Tg
E
cumulative fraction (%)
0
1
2
3
4
5
6
inter-event interval (s)
WT
Tg
(HZ)
2.0
1.5
1.0
0.5
0
WT
Tg
F
WT
Tg
G
cumulative fraction (%)
50
100
150
200
amplitude (dA)
WT
Tg
(pA)
30
20
10
0
WT
Tg
H
cumulative fraction (%)
0
500
1000
1500
inter-event interval (ms)
WT
Tg
(HZ)
8
6
4
2
0
WT
Tg

◂**Fig. 3** Tg mice show enhanced LTP but not excitatory/inhibitory neurotransmission. **A** Time-course of fEPSP in CA1 neurons of WT ($n = 6$) and Tg mice ($n = 6$). LTP is induced after high-frequency stimulation (HFS; 100 Hz for 1 s) at the indicated time by the arrow. Representative traces of the fEPSP before (1) and 1 h after (2) HFS are shown on the top. Scale bar: 0.5 mV/10 ms. **B** Bar graphs comparing LTP observed during the last 10 min in WT and Tg mice (data were analyzed by Student's *t* test; $n = 6/6$ mice. Error bars are SEM; $^*P < 0.05$). **C**–**H** Representative trace of mEPSC (**C**) or mIPSC (**F**) of WT and Tg mice in CA1 pyramidal cells, scale bar: 10 pA/5 s. Cumulative fractions and bar plots (insets) of mEPSC (**D**, **E**) or mIPSC (**G**, **H**) amplitude and frequency (inter-event intervals) in WT and Tg mice (data were analyzed by Student's *t* test; $n = 6/6$ mice. Error bars are SEM)

increased, both in the hippocampus and cortex of Tg mice ($P < 0.05$ in each group, Fig. 5A–D). Although CaMKII has been implicated in LTP and spatial learning [39, 40], CaMKII activity defined by the ratio of p-CaMKII/CaMKII was not significantly changed in Tg mice (Fig. 5A–D). These results suggested that BDNF and downstream signaling molecules ERK and CREB play a key role in learning and memory of Tg mice.

LTP induction was decreased by CREB knockdown and anti-BDNF antibody in Tg mice

To further test whether direct manipulation of CREB may affect learning and memory of Tg mice, we assessed the LTP in WT and Tg mice when *CREB* gene was knocked down. Western blotting analysis showed that the expression of CREB was significantly decreased in all mice treated with lenti-shCREB compared with vector containing scrambled sequence (lenti-scr, $P < 0.01$, Fig. 6A), indicating that the lentiviral vector was successfully delivered. As shown in Fig. 6B, LTP amplitude was significantly decreased in Tg mice treated with lenti-shCREB (Tg-lenti-shCREB) compared with lenti-scr (164.4 ± 1.46% in Tg-lenti-scr; 146.9 ± 1.33% in Tg-lenti-shCREB, $P < 0.01$, data were taken from the last 10 min of recording, Fig. 6C), whereas WT-lenti-shCREB did not cause changes of fEPSP compared with WT-lenti-scr, indicating that *CREB* knockdown reduced hippocampal LTP induction in Furin-Tg mice rather than under basal condition.

To determine whether furin enhancement of LTP was mediated by BDNF, we assessed LTP in the hippocampus of Tg mice bilaterally injected with anti-BDNF antibody. As

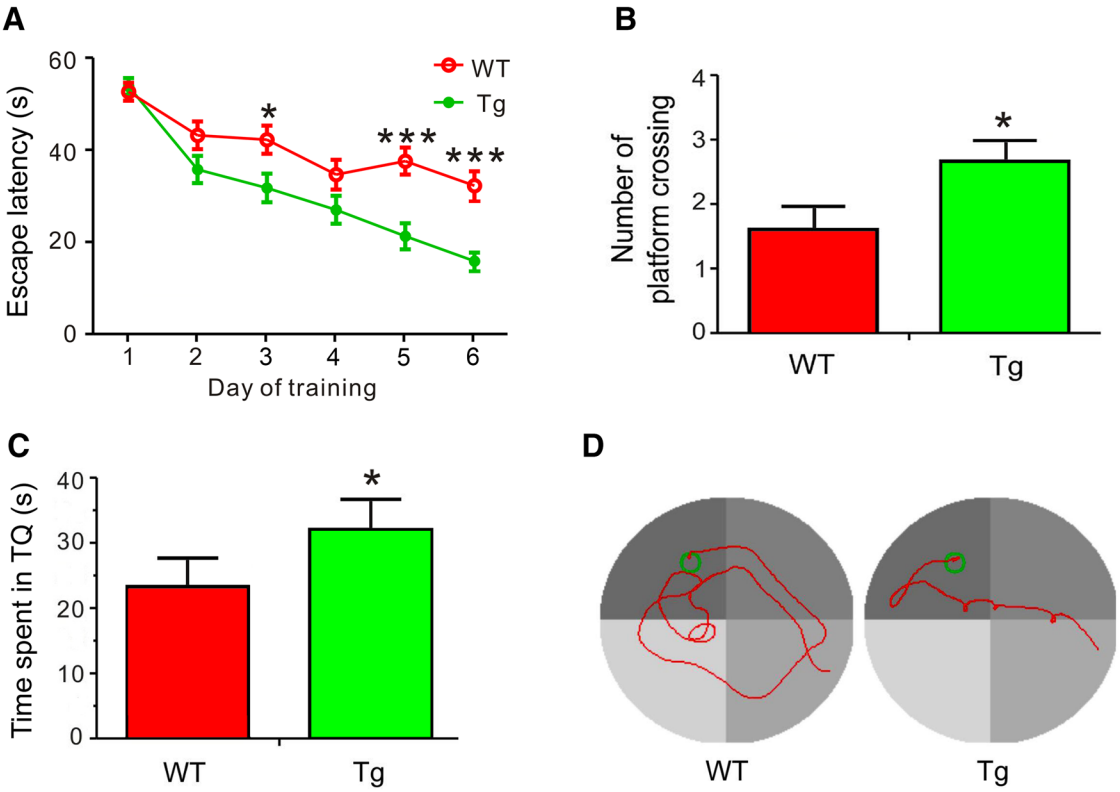

Fig. 4 Spatial learning and memory performance are improved in Tg mice. Morris water maze test showing the mean escape latency from day 1 to 6 (**A**), the number of crossing (**B**) and the time spent in target quadrant (TQ) (**C**) (data were analyzed by Student's *t* test; $n = 14$ in each group. Error bars are SEM; $^*P < 0.05$, $^{***}P < 0.001$). **D** Typical pathlengths showing the movement trajectory of mice in hidden platform experiment on the fifth day. The circle represents the previous location of the platform

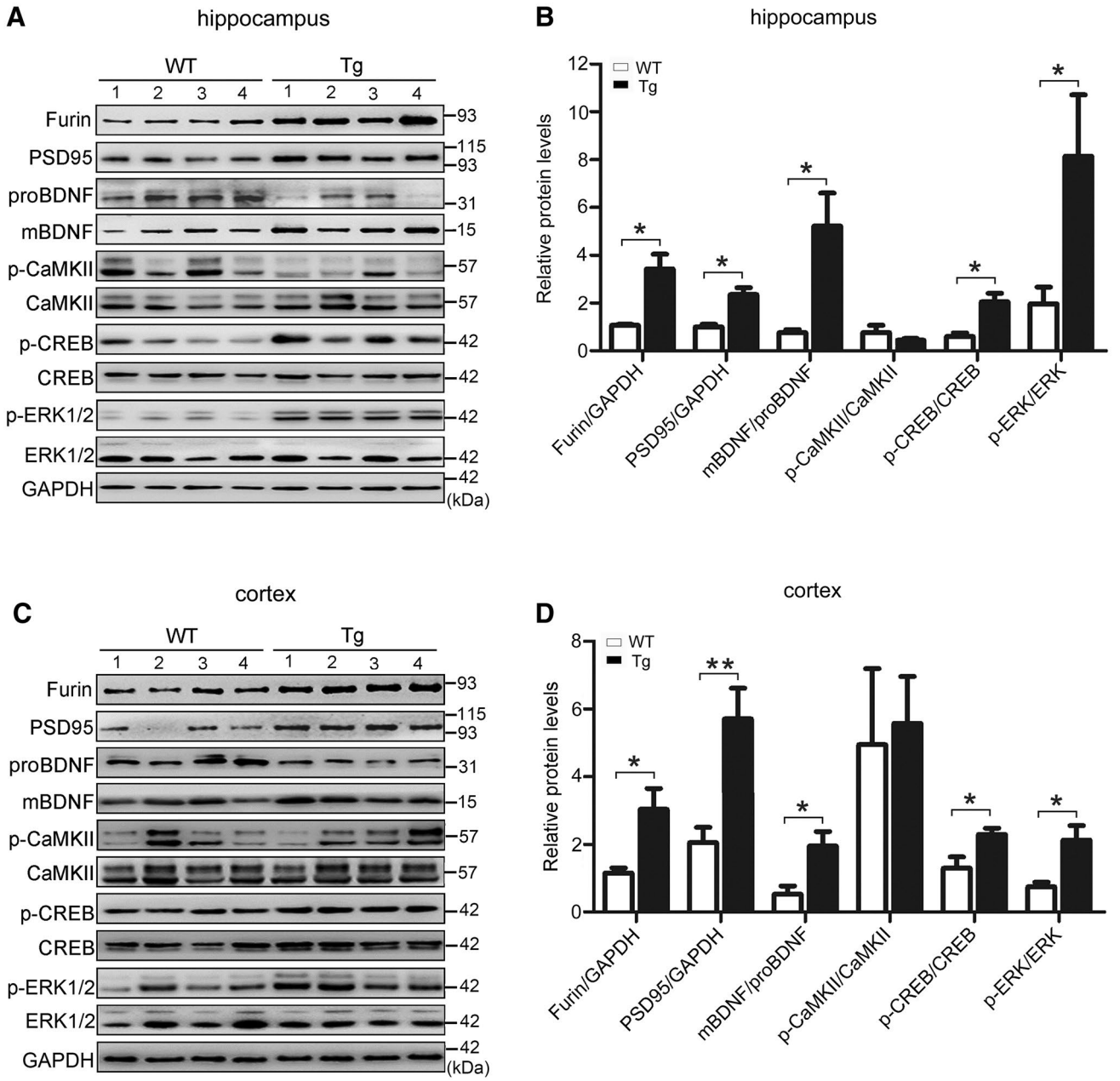

Fig. 5 Furin-associated proteins are altered in Tg mice. Representative Western blots (**A**) and quantitative analysis (**B**) of furin-related proteins in the hippocampus of WT and Tg mice, respectively (data were analyzed by Student's *t* test; $n = 8$ in each group. Error bars are SEM; $^*P < 0.05$). The molecular weight of protein marker in kDa is shown to the right of each Western blot panel. Representative Western blots (**C**) and quantitative analysis (**D**) of furin-related proteins in the cortex of WT and Tg mice, respectively (data were analyzed by Student's *t* test; $n = 8$ in each group. Error bars are SEM; $^*P < 0.05$, $^{**}P < 0.01$). The molecular weight of protein marker in kDa is shown to the right of each Western blot panel

shown in Fig. 6D, E, BDNF antibody significantly inhibited LTP, compared with control IgG (last 10 min of recording, anti-IgG, 158.9 ± 2.00%; anti-BDNF, 136.2 ± 3.38%, $n = 6/6$ mice, $P < 0.01$). Consistently, inhibition of BDNF signaling by BDNF antibody also led to significantly reduced p-CREB level relative to control IgG ($P < 0.01$, Fig. 6F). These results suggested that the blockade of BDNF function through anti-BDNF antibody injection in the hippocampus of Tg mice reduces the enhanced LTP.

CREB knockdown reduced cognitive improvement in Tg mice

We then investigated the effect of *CREB* knockdown on spatial learning and memory in WT and Tg mice. The escape latency in Tg-lenti-shCREB mice was significantly higher than that in Tg-lenti-scr mice from day 2 to day 6 ($P < 0.05$, Fig. 7A). In the probe trials when the platform was removed, the time stayed in TQ was significantly shorter in Tg-lenti-shCREB mice than that in Tg-lenti-scr mice (19.48 ± 4.75 s in Tg-lenti-shCREB and 29.13 ± 4.28 s in Tg-lenti-scr; $P < 0.05$, Fig. 7B). However, the passing times crossing over target site (number of platform crossing) was comparable between these mice (1.72 ± 0.52 in Tg-lenti-shCREB and 1.89 ± 0.48 in Tg-lenti-scr; $P > 0.05$, Fig. 7C). No significant difference was observed between Tg-lenti-shCREB and WT mice (WT-lenti-shCREB, WT-lenti-scr) in escape latency (Fig. 7A), staying time (Fig. 7B) and passing times (Fig. 7C), respectively. Representative probe trial trajectories for both groups are shown (Fig. 7D), illustrating inferior learning performance in Tg-lenti-shCREB mice. These results suggested that CREB activity was involved in furin-mediated enhancement of cognitive function.

Discussion

In the present study, we have found that furin promotes spine morphogenesis, LTP and spatial memory. These changes are consistent with the increased mBDNF formation and downstream ERK and CREB activities in the brain. Moreover, *CREB* knockdown reduces furin-mediated electrical and behavioral effects. Thus, our study provides evidence that in mammals, furin facilitates learning and memory through CREB-dependent mechanisms.

Dendritic spine morphogenesis involves an array of factors [41]. In addition to the activity-dependent activation of NMDAR and AMPAR, BDNF seems to play a role in triggering actin rearrangement and spine growth [29]. In line with this, BDNF increases synaptic spine density in CA1 pyramidal neurons without affecting dendritic branching [42]. In a mouse model of autism, deregulation of BDNF signaling also influences spine morphogenesis [43]. It is worth noting that pro-BDNF and its receptor $p75^{NTR}$ negatively regulate spine density, and this effect is rescued by $p75^{NTR}$ antibody [44, 45]. In our study, the elevated spine density in Tg mice is consistent with the increased ratio of mBDNF over pro-BDNF, as well as the spine density marker PSD95 [46], supporting the role of BDNF in furin enhancement of spine density. However, BDNF may not be the only one substrate of furin that promotes neurogenesis [27]. It is reported that Notch1, another furin substrates involved in neurogenesis [47, 48], is required for hypoxia-induced spine morphogenesis in the hippocampus [49].

LTP can be categorized into three forms, LTP1, LTP2 and LTP3, which may be associated with discrete mechanisms [34]. LTP1 and LTP2 are short-lasting (1–3 h) and are dependent on post-translational and translational modification of synaptic proteins, respectively. LTP3 lasts for hours to weeks and is both translation- and transcription-dependent [50]. While AMPAR, NMDAR and CAMKII are actively involved in short-lasting of LTP, CREB activation associated with gene transcription may play more important role in long-lasting LTP [34]. Interestingly, these mechanisms seem to be closely associated with BDNF, as it is well-documented that BDNF regulates NMDAR and AMPAR as well as LTP [12, 51]. However, it should be noted that BDNF effect on neurotransmission differs in time and experimental condition. Acute application of BDNF potentiates mEPSC and mIPSC [52]. In cultured neurons, chronic administration of BDNF (100 ng/mL) increased mEPSC amplitude, whereas TrKB-IgG was without effect [53, 54]. It is also reported that in $BDNF^{+/-}$ mice, mEPSC was not altered whereas LTP is abolished in brain slices [55], which may be more relevant to our in vivo experimental conditions. In line with this, the amplitude and frequency of mEPSC/mIPSC are not altered in our study, and CaMKII activity also remains unchanged (Figs. 3, 5). The long-term effect of BDNF has been demonstrated in BDNF- or TrkB-KO mice, in which dendritic translation of proteins promoting cellular process of memory consolidation has been suggested [56–58]. The role of BDNF in LTP has been well-documented [14, 51]. BDNF exerts its biological function upon binding to tyrosine kinase receptor B (TrkB), which initiates intracellular signaling cascades, including ERK and CREB activation [35, 59–61]. ERK activation is known to be closely associated with LTP [62, 63], while CREB is targeted by ERK in controlling LTP-dependent gene transcription [64, 65]. Therefore, CREB activation that is associated with BDNF seems to be essential for furin regulation of LTP. This assumption is supported by the following findings in our study: (1) the ratio of mBDNF to pro-BDNF is significantly elevated in the brain of Tg mice, indicating that furin effectively exerts the proprotein convertase activity [8, 66]; (2) BDNF downstream signaling ERK and CREB are activated, as revealed by the increased p-ERK and p-CREB levels; (3) inhibition of BDNF signaling by BDNF antibody attenuated LTP and p-CREB in Tg mice, and (4) hippocampal knockdown of CREB reduces furin-mediated LTP induction and cognitive enhancement.

The role of CREB in LTP and memory has been intensively investigated [67]. CREB knockdown does not alter LTP in hippocampal slices under basal condition, and the slight alteration of spatial memory does not occur in the consecutive recording for 11 days until the 12th day [68].

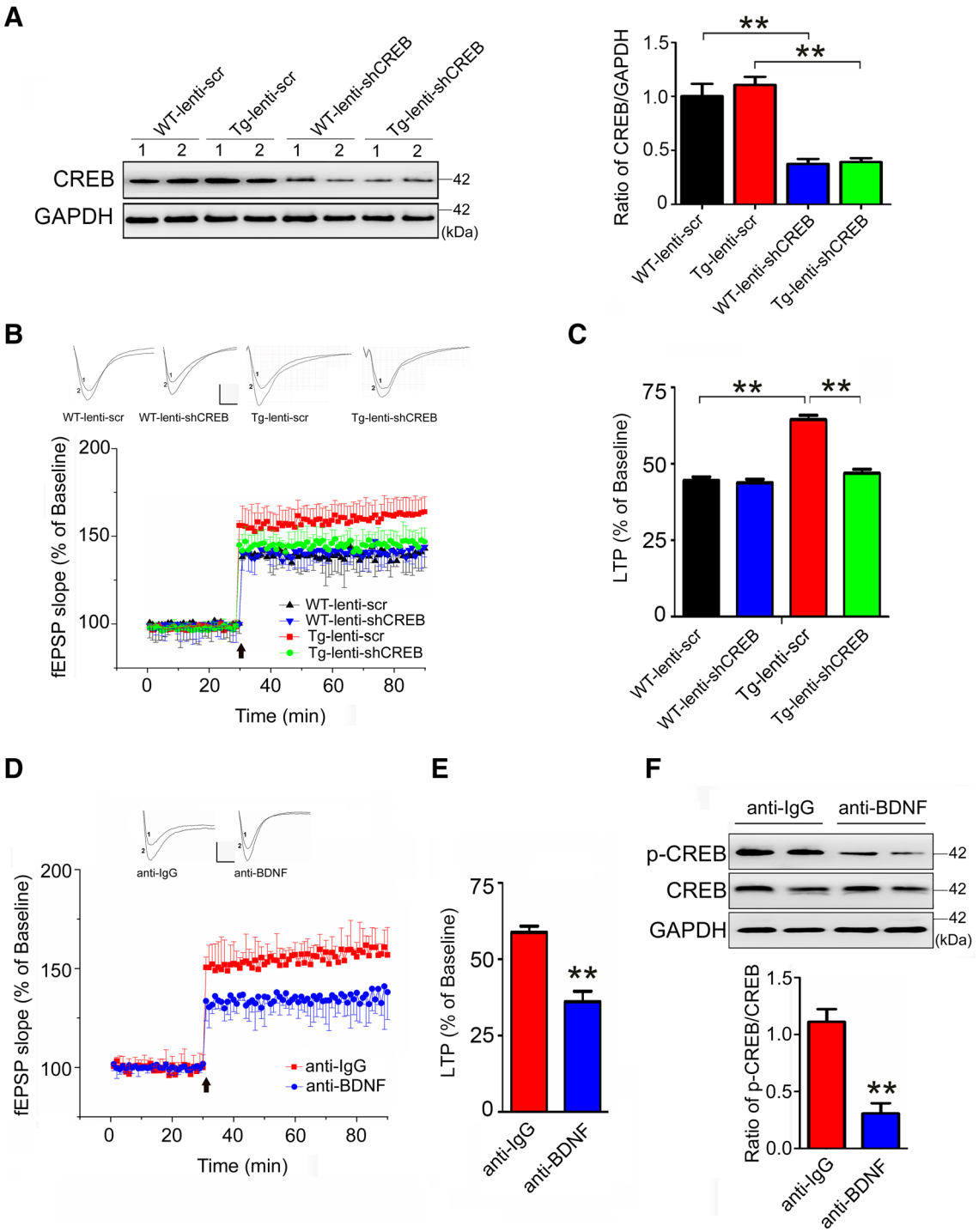

Interestingly, this same study reveals that CREB knockdown prevents PKA agonist forskolin- and dopamine D1 agonist chlo-APB-induced LTP [68]. It seems that CREB may alternatively affect LTP-associated mechanism in primed condition. In line with this, CREB antisense is found to prevent estrogen-induced spine formation in cultured neurons [69]. In Aplysia sensory neurons, serotonin-induced long-term facilitation is dependent on CREB [70]. It is reported that CREB is considered as a major mediator of BDNF signaling [71]. It seems that CREB may alternatively affect LTP-associated mechanism in "primed" condition. The primed condition may be resembled by the enhanced level of mBDNF in Furin-Tg mice but not in WT mice in our study; in Tg mice CREB knockdown leads to the attenuated LTP and cognitive function.

◂**Fig. 6** CREB knockdown and anti-BDNF antibody inhibit LTP in Tg mice. **A** CREB protein levels in the hippocampus of WT and Tg mice injected with lentivirus bearing scrambled sequence (WT-lenti-scr, Tg-lenti-scr mice, $n = 8$) or shCREB (WT-lenti-shCREB, Tg-lenti-shCREB, $n = 9$) (data were analyzed by Student's t test; error bars are SEM; $^{**}P < 0.01$). The molecular weight of protein marker in kDa is shown to the right of each Western blot panel. **B** Time-course of fEPSP in CA1 neurons of WT and Tg mice treated with lenti-scr and lenti-shCREB. LTP is induced after high-frequency stimulation (HFS; 100 Hz for 1 s). Representative traces of the fEPSP before (1) and 1 h after (2) HFS are shown on the top. Scale bar: 0.5 mV/10 ms. **C** Bar graphs comparing LTP during the last 10 min in Tg-lenti-shCREB ($n = 9$), WT-lenti-shCREB ($n = 9$), Tg-lenti-scr ($n = 8$) and WT-lenti-scr mice ($n = 8$) (data were analyzed by Student's t test; error bars are SEM; $^{**}P < 0.01$). **D** Time-course of fEPSP in CA1 neurons of Tg mice injection with control rabbit IgG (anti-IgG, $n = 6$) and BDNF antibody (anti-BDNF, $n = 6$). LTP is induced after high-frequency stimulation (HFS; 100 Hz for 1 s). Representative traces of the fEPSP before (1) and 1 h after (2) HFS are shown on the top. Scale bar: 0.5 mV/10 ms. **E** Bar graphs comparing LTP during the last 10 min in anti-IgG and anti-BDNF mice. Data were analyzed by Student's t test; $n = 6/6$ mice. Error bars are SEM; $^{**}P < 0.01$. **F** Representative Western blots and quantitative analysis of p-CREB protein in the hippocampus of Tg mice injected with either IgG ($n = 6$) or antibody to BDNF ($n = 6$) (data were analyzed by Student's t test; error bars are SEM; $^{**}P < 0.01$). The molecular weight of protein marker in kDa is shown to the right of each Western blot panel

Dendritic morphogenesis and LTP induction may be related to each other. Protein synthesis in dendrites plays a critical role in LTP induction, which requires actin dynamics and translation of local mRNA [56, 72]. Defect of actin-binding protein synaptopodin in the spine apparatus results in impaired LTP [50]. Knockdown of PSD95, a well-known determinant of PSD size and synaptic strength, blocks LTP in superior colliculus [73–75]. Conversely, chemical or electrical LTP-generating stimulations lead to spines to rapidly expand and the formation of new spines [41]. Evidence has suggested that these processes are closely related to BDNF signaling [76]. For instance, BDNF injection induces stable LTP and enhanced hippocampal cell proliferation exhibited by increased $BrdU^+$ cell numbers [27]. PSD95 is among those translocated to dendritic spines by BDNF [77]. BDNF-induced dendritic morphogenesis is critically dependent on ERK and actin dynamics [42]. CREB activation, an essential step in the cascade of new dendritic spines during LTP [69, 78], is responsible for BDNF regulation of LTP [71]. It is tempting to speculate that the elevated formation of mBDNF catalyzed by furin is a key step, which leads to dendritic morphogenesis and LTP induction, resulting in the enhancement of cognitive function.

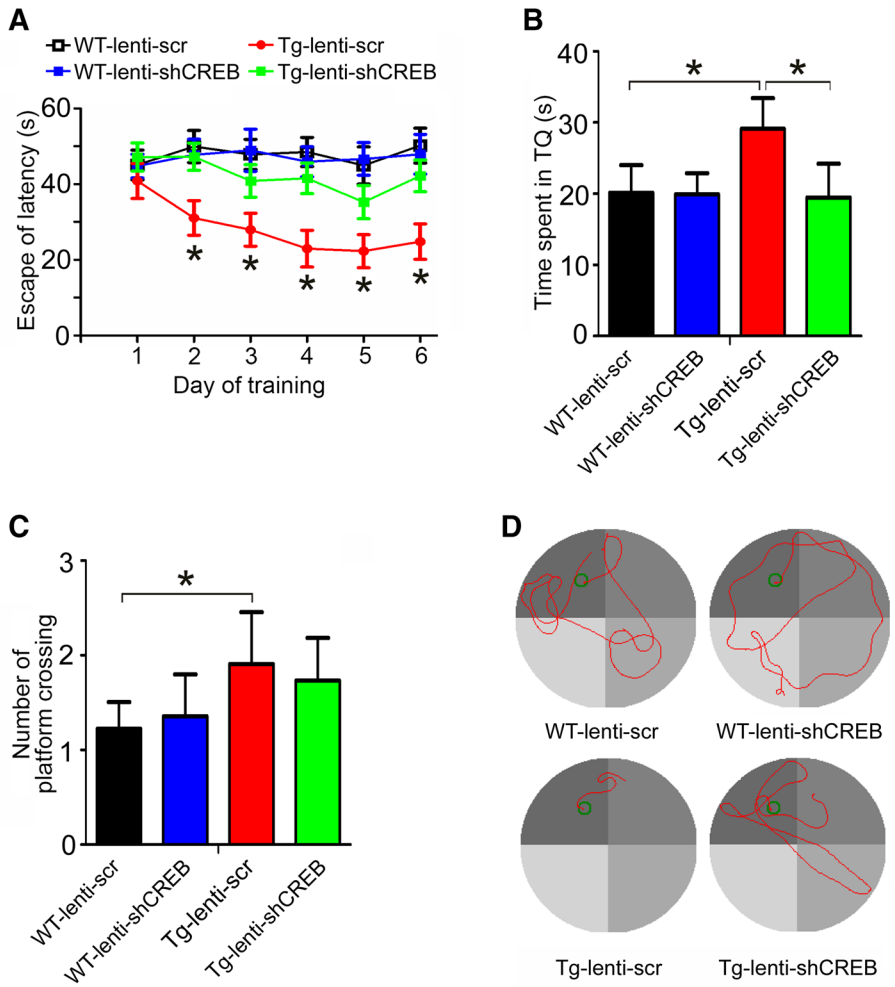

Fig. 7 CREB knockdown inhibits cognitive function in Tg mice. Morris water maze test showing the mean escape latency from day 1 to 6 (**A**), time spent in the target quadrant (**B**) and the number of crossing (**C**) (data were analyzed by Student's t test; $n = 14$ in each group. Error bars are SEM; $^{*}P < 0.05$). **D** Typical path-lengths showing the movement trajectory of mice in hidden platform experiment on the fifth day. The circle represents the previous location of the platform

In our study, the role of NMDAR and AMPAR in spine density and LTP seems to be dispensable, as mEPSC and mIPSC remain unchanged. Alternatively, we have identified that CREB is a critical mediator, as hippocampal knockdown of CREB reduces furin regulation of LTP and spatial memory. This could be attributed to, at least in part, the increased mBDNF formation relative to the catalytic activity of furin. However, the current study does not exclude the involvement of other furin substrates including Notch1. Nonetheless, furin expression is decreased in the brain of patients with Alzheimer's disease (AD), in which mBDNF/pro-BDNF ratio is decreased [79]. The molecular mechanisms associated with furin regulation of learning and memory may provide new insight into the understanding and treatment strategy of neurological diseases such as AD.

Acknowledgements This work was supported by the National Natural Science Foundation of China (81220108010 to G.-J. Chen; 31500821 to B.-L. Zhu; 81622015 and 81571042 to Z.-F. Dong).

Author contributions B-LZ and G-JC designed the experiments. B-LZ, L-GZ, YT, ZM and D-MX performed the experiments and the statistical analysis. B-L Zhu and G-J Chen wrote the manuscript. All authors contributed to preparation of the manuscript and approved the final contributions.

Compliance with ethical standards

Conflict of interest The authors declare no conflicts of interest.

References

1. Thomas G (2002) Furin at the cutting edge: from protein traffic to embryogenesis and disease. Nat Rev Mol Cell Biol 3:753–766
2. Nakayama K (1997) Furin: a mammalian subtilisin/Kex2p-like endoprotease involved in processing of a wide variety of precursor proteins. Biochem J 327(Pt 3):625–635
3. Scamuffa N, Calvo F, Chretien M, Seidah NG, Khatib AM (2006) Proprotein convertases: lessons from knockouts. FASEB J 20:1954–1963
4. Schroeder NE, Androwski RJ, Rashid A, Lee H, Lee J et al (2013) Dauer-specific dendrite arborization in *C. elegans* is regulated by KPC-1/Furin. Curr Biol 23:1527–1535
5. Salzberg Y, Ramirez-Suarez NJ, Bulow HE (2014) The proprotein convertase KPC-1/furin controls branching and self-avoidance of sensory dendrites in *Caenorhabditis elegans*. PLoS Genet 10:e1004657
6. Seidah NG, Benjannet S, Pareek S, Chretien M, Murphy RA (1996) Cellular processing of the neurotrophin precursors of NT3 and BDNF by the mammalian proprotein convertases. FEBS Lett 379:247–250
7. Yang M, Lim Y, Li X, Zhong JH, Zhou XF (2011) Precursor of brain-derived neurotrophic factor (proBDNF) forms a complex with Huntingtin-associated protein-1 (HAP1) and sortilin that modulates proBDNF trafficking, degradation, and processing. J Biol Chem 286:16272–16284
8. Chen Y, Zhang J, Deng M (2015) Furin mediates brain-derived neurotrophic factor upregulation in cultured rat astrocytes exposed to oxygen-glucose deprivation. J Neurosci Res 93:189–194
9. Cao J, Tang Y, Li Y, Gao K, Shi X et al (2017) Behavioral changes and hippocampus glucose metabolism in APP/PS1 transgenic mice via electro-acupuncture at governor vessel acupoints. Front Aging Neurosci 9:5
10. Lu B, Nagappan G, Guan X, Nathan PJ, Wren P (2013) BDNF-based synaptic repair as a disease-modifying strategy for neurodegenerative diseases. Nat Rev Neurosci 14:401–416
11. Mizui T, Ishikawa Y, Kumanogoh H, Kojima M (2016) Neurobiological actions by three distinct subtypes of brain-derived neurotrophic factor: multi-ligand model of growth factor signaling. Pharmacol Res 105:93–98
12. Zagrebelsky M, Korte M (2014) Form follows function: BDNF and its involvement in sculpting the function and structure of synapses. Neuropharmacology 76 Pt C:628–638
13. Lipsky RH, Marini AM (2007) Brain-derived neurotrophic factor in neuronal survival and behavior-related plasticity. Ann N Y Acad Sci 1122:130–143
14. Leal G, Bramham CR, Duarte CB (2017) BDNF and hippocampal synaptic plasticity. Vitam Horm 104:153–195
15. Pastalkova E, Serrano P, Pinkhasova D, Wallace E, Fenton AA et al (2006) Storage of spatial information by the maintenance mechanism of LTP. Science 313:1141–1144
16. Whitlock JR, Heynen AJ, Shuler MG, Bear MF (2006) Learning induces long-term potentiation in the hippocampus. Science 313:1093–1097
17. Borchelt DR, Davis J, Fischer M, Lee MK, Slunt HH et al (1996) A vector for expressing foreign genes in the brains and hearts of transgenic mice. Genet Anal 13:159–163
18. Fujimori K, Yano M, Miyake H, Kimura H (2014) Termination mechanism of CREB-dependent activation of COX-2 expression in early phase of adipogenesis. Mol Cell Endocrinol 384:12–22
19. Zhang Y, Chen G, Gao B, Li Y, Liang S et al (2016) NR4A1 knockdown suppresses seizure activity by regulating surface expression of NR2B. Sci Rep 6:37713
20. Chen DY, Bambah-Mukku D, Pollonini G, Alberini CM (2012) Glucocorticoid receptors recruit the CaMKIIalpha–BDNF–CREB pathways to mediate memory consolidation. Nat Neurosci 15:1707–1714
21. Bambah-Mukku D, Travaglia A, Chen DY, Pollonini G, Alberini CM (2014) A positive autoregulatory BDNF feedback loop via C/EBPbeta mediates hippocampal memory consolidation. J Neurosci 34:12547–12559
22. Alonso M, Vianna MR, Izquierdo I, Medina JH (2002) Signaling mechanisms mediating BDNF modulation of memory formation in vivo in the hippocampus. Cell Mol Neurobiol 22:663–674
23. Hu XT, Zhu BL, Zhao LG, Wang JW, Liu L et al (2017) Histone deacetylase inhibitor apicidin increases expression of the alpha-secretase ADAM10 through transcription factor USF1-mediated mechanisms. FASEB J 31:1482–1493
24. Moghaddam M, Bures J (1997) Rotation of water in the Morris water maze interferes with path integration mechanisms of place navigation. Neurobiol Learn Mem 68:239–251
25. Tang B, Luo D, Yang J, Xu XY, Zhu BL et al (2015) Modulation of AMPA receptor mediated current by nicotinic acetylcholine receptor in layer I neurons of rat prefrontal cortex. Sci Rep 5:14099
26. Mathis DM, Furman JL, Norris CM (2011) Preparation of acute hippocampal slices from rats and transgenic mice for the study of synaptic alterations during aging and amyloid pathology. J Vis Exp 23:2330

27. Kuipers SD, Trentani A, Tiron A, Mao X, Kuhl D et al (2016) BDNF-induced LTP is associated with rapid Arc/Arg3.1-dependent enhancement in adult hippocampal neurogenesis. Sci Rep 6:21222
28. Tada T, Sheng M (2006) Molecular mechanisms of dendritic spine morphogenesis. Curr Opin Neurobiol 16:95–101
29. Lai KO, Ip NY (2013) Structural plasticity of dendritic spines: the underlying mechanisms and its dysregulation in brain disorders. Biochim Biophys Acta 1832:2257–2263
30. Wang B, Wang Z, Sun L, Yang L, Li H et al (2014) The amyloid precursor protein controls adult hippocampal neurogenesis through GABAergic interneurons. J Neurosci 34:13314–13325
31. Kneussel M, Hausrat TJ (2016) Postsynaptic neurotransmitter receptor reserve pools for synaptic potentiation. Trends Neurosci 39:170–182
32. Deng-Bryant Y, Leung LY, Caudle K, Tortella F, Shear D (2016) Cognitive evaluation using morris water maze in neurotrauma. Methods Mol Biol 1462:539–551
33. Lynch MA (2004) Long-term potentiation and memory. Physiol Rev 84:87–136
34. Raymond CR (2007) LTP forms 1, 2 and 3: different mechanisms for the "long" in long-term potentiation. Trends Neurosci 30:167–175
35. Ehrlich DE, Josselyn SA (2016) Plasticity-related genes in brain development and amygdala-dependent learning. Genes Brain Behav 15:125–143
36. Ying SW, Futter M, Rosenblum K, Webber MJ, Hunt SP et al (2002) Brain-derived neurotrophic factor induces long-term potentiation in intact adult hippocampus: requirement for ERK activation coupled to CREB and upregulation of Arc synthesis. J Neurosci 22:1532–1540
37. Posada-Duque RA, Ramirez O, Hartel S, Inestrosa NC, Bodaleo F et al (2017) CDK5 downregulation enhances synaptic plasticity. Cell Mol Life Sci 74:153–172
38. Gao H, Yan P, Zhang S, Huang H, Huang F et al (2016) Long-term dietary alpha-linolenic acid supplement alleviates cognitive impairment correlate with activating hippocampal CREB signaling in natural aging rats. Mol Neurobiol 53:4772–4786
39. Shonesy BC, Jalan-Sakrikar N, Cavener VS, Colbran RJ (2014) CaMKII: a molecular substrate for synaptic plasticity and memory. Prog Mol Biol Transl Sci 122:61–87
40. Murakoshi H, Shin ME, Parra-Bueno P, Szatmari EM, Shibata AC et al (2017) Kinetics of endogenous CaMKII required for synaptic plasticity revealed by optogenetic kinase inhibitor. Neuron 94(37–47):e35
41. Segal M (2017) Dendritic spines: morphological building blocks of memory. Neurobiol Learn Mem 138:3–9
42. Alonso M, Medina JH, Pozzo-Miller L (2004) ERK1/2 activation is necessary for BDNF to increase dendritic spine density in hippocampal CA1 pyramidal neurons. Learn Mem 11:172–178
43. Huber KM, Klann E, Costa-Mattioli M, Zukin RS (2015) Dysregulation of mammalian target of rapamycin signaling in mouse models of autism. J Neurosci 35:13836–13842
44. Koshimizu H, Kiyosue K, Hara T, Hazama S, Suzuki S et al (2009) Multiple functions of precursor BDNF to CNS neurons: negative regulation of neurite growth, spine formation and cell survival. Mol Brain 2:27
45. Zagrebelsky M, Holz A, Dechant G, Barde YA, Bonhoeffer T et al (2005) The p75 neurotrophin receptor negatively modulates dendrite complexity and spine density in hippocampal neurons. J Neurosci 25:9989–9999
46. Ebrahimi S, Okabe S (2014) Structural dynamics of dendritic spines: molecular composition, geometry and functional regulation. Biochim Biophys Acta 1838:2391–2398
47. Caviness VS Jr, Nowakowski RS, Bhide PG (2009) Neocortical neurogenesis: morphogenetic gradients and beyond. Trends Neurosci 32:443–450
48. Tiyanont K, Wales TE, Aste-Amezaga M, Aster JC, Engen JR et al (2011) Evidence for increased exposure of the Notch1 metalloprotease cleavage site upon conversion to an activated conformation. Structure 19:546–554
49. Zhang K, Zhao T, Huang X, Wu LY, Wu K et al (2014) Notch1 mediates postnatal neurogenesis in hippocampus enhanced by intermittent hypoxia. Neurobiol Dis 64:66–78
50. Jedlicka P, Vlachos A, Schwarzacher SW, Deller T (2008) A role for the spine apparatus in LTP and spatial learning. Behav Brain Res 192:12–19
51. Bekinschtein P, Cammarota M, Medina JH (2014) BDNF and memory processing. Neuropharmacology 76 Pt C:677–683
52. Bramham CR, Messaoudi E (2005) BDNF function in adult synaptic plasticity: the synaptic consolidation hypothesis. Prog Neurobiol 76:99–125
53. Sherwood NT, Lo DC (1999) Long-term enhancement of central synaptic transmission by chronic brain-derived neurotrophic factor treatment. J Neurosci 19:7025–7036
54. Bolton MM, Lo DC, Sherwood NT (2000) Long-term regulation of excitatory and inhibitory synaptic transmission in hippocampal cultures by brain-derived neurotrophic factor. Prog Brain Res 128:203–218
55. Meis S, Endres T, Lessmann V (2012) Postsynaptic BDNF signalling regulates long-term potentiation at thalamo-amygdala afferents. J Physiol 590:193–208
56. Bramham CR (2008) Local protein synthesis, actin dynamics, and LTP consolidation. Curr Opin Neurobiol 18:524–531
57. Korte M, Kang H, Bonhoeffer T, Schuman E (1998) A role for BDNF in the late-phase of hippocampal long-term potentiation. Neuropharmacology 37:553–559
58. Minichiello L, Korte M, Wolfer D, Kühn R, Unsicker K et al (1999) Essential role for TrkB receptors in hippocampus-mediated learning. Neuron 24:401–414
59. Tyler WJ, Alonso M, Bramham CR, Pozzo-Miller LD (2002) From acquisition to consolidation: on the role of brain-derived neurotrophic factor signaling in hippocampal-dependent learning. Learn Mem 9:224–237
60. Lonze BE, Ginty DD (2002) Function and regulation of CREB family transcription factors in the nervous system. Neuron 35:605–623
61. Sakamoto K, Karelina K, Obrietan K (2011) CREB: a multifaceted regulator of neuronal plasticity and protection. J Neurochem 116:1–9
62. English JD, Sweatt JD (1997) A requirement for the mitogen-activated protein kinase cascade in hippocampal long term potentiation. J Biol Chem 272:19103–19106
63. Gooney M, Shaw K, Kelly A, O'Mara SM, Lynch MA (2002) Long-term potentiation and spatial learning are associated with increased phosphorylation of TrkB and extracellular signal-regulated kinase (ERK) in the dentate gyrus: evidence for a role for brain-derived neurotrophic factor. Behav Neurosci 116:455–463
64. Davis S, Vanhoutte P, Pages C, Caboche J, Laroche S (2000) The MAPK/ERK cascade targets both Elk-1 and cAMP response element-binding protein to control long-term potentiation-dependent gene expression in the dentate gyrus in vivo. J Neurosci 20:4563–4572
65. Impey S, Obrietan K, Wong ST, Poser S, Yano S et al (1998) Cross talk between ERK and PKA is required for Ca2 + stimulation of CREB-dependent transcription and ERK nuclear translocation. Neuron 21:869–883
66. Wetsel WC, Rodriguiz RM, Guillemot J, Rousselet E, Essalmani R et al (2013) Disruption of the expression of the proprotein

convertase PC7 reduces BDNF production and affects learning and memory in mice. Proc Natl Acad Sci USA 110:17362–17367
67. Barco A, Marie H (2011) Genetic approaches to investigate the role of CREB in neuronal plasticity and memory. Mol Neurobiol 44:330–349
68. Pittenger C, Huang YY, Paletzki RF, Bourtchouladze R, Scanlin H et al (2002) Reversible inhibition of CREB/ATF transcription factors in region CA1 of the dorsal hippocampus disrupts hippocampus-dependent spatial memory. Neuron 34:447–462
69. Murphy DD, Segal M (1997) Morphological plasticity of dendritic spines in central neurons is mediated by activation of cAMP response element binding protein. Proc Natl Acad Sci USA 94:1482–1487
70. Casadio A, Martin KC, Giustetto M, Zhu H, Chen M et al (1999) A transient, neuron-wide form of CREB-mediated long-term facilitation can be stabilized at specific synapses by local protein synthesis. Cell 99:221–237
71. Finkbeiner S, Tavazoie SF, Maloratsky A, Jacobs KM, Harris KM et al (1997) CREB: a major mediator of neuronal neurotrophin responses. Neuron 19:1031–1047
72. Yang Y, Zhou Q (2009) Spine modifications associated with long-term potentiation. Neuroscientist 15:464–476
73. Wang Z, Yan P, Hui T, Zhang J (2014) Epigenetic upregulation of PSD-95 contributes to the rewarding behavior by morphine conditioning. Eur J Pharmacol 732:123–129
74. Xu W (2011) PSD-95-like membrane associated guanylate kinases (PSD-MAGUKs) and synaptic plasticity. Curr Opin Neurobiol 21:306–312
75. Zhao JP, Murata Y, Constantine-Paton M (2013) Eye opening and PSD95 are required for long-term potentiation in developing superior colliculus. Proc Natl Acad Sci USA 110:707–712
76. Leal G, Afonso PM, Salazar IL, Duarte CB (2015) Regulation of hippocampal synaptic plasticity by BDNF. Brain Res 1621:82–101
77. Butko MT, Yang J, Geng Y, Kim HJ, Jeon NL et al (2012) Fluorescent and photo-oxidizing TimeSTAMP tags track protein fates in light and electron microscopy. Nat Neurosci 15:1742–1751
78. Ortega-Martinez S (2015) A new perspective on the role of the CREB family of transcription factors in memory consolidation via adult hippocampal neurogenesis. Front Mol Neurosci 8:46
79. Keifer J, Zheng Z, Ambigapathy G (2015) A microRNA-BDNF negative feedback signaling loop in brain: implications for Alzheimer's disease. Microrna 4:101–108